Anisotropic spin-crossover composite actuators displaying pre-programmed movements

Mario Piedrahita-Bello, Xinyu Yang, Seyed Ehsan Alavi, Gábor Molnár, L. Salmon, Azzedine Bousseksou

Anisotropic Spin-Crossover Composite Actuators Displaying Pre-Programmed Movements

Mario Piedrahita-Bello, Xinyu Yang, Seyed Ehsan Alavi, Gábor Molnár, Lionel Salmon,* Azzedine Bousseksou*

LCC, CNRS & Université de Toulouse (UPS, INP), 31077 Toulouse, France

* lionel.salmon@lcc-toulouse.fr, azzedine.bousseksou@lcc-toulouse.fr

Abstract

In this work, we propose shape-morphing electro-thermal actuators, which can realize various pre-programmed movements, such as large-strain bending or helical curling. The bimorph actuators consist of an electrically conducting polymer composite layer, used for Joule heating, and a spin-crossover polymer composite layer, which affords for a large thermal strain. By using needle-shaped spin crossover particles and adjusting their orientation with respect to the two axes of the T-shaped actuator, the deformation of each device can be encoded in a predictable manner. Based on mechanical property measurements and associated finite element analysis we show that the observed movements are governed primarily by the anisotropy of the transformation strain generated by the spin crossover particles. We envision that this type of self-folding structures can be advantageously used in remote and small-scale mechanical applications.

Introduction

In the past decades, stimuli-responsive materials have attracted much interest for developing shape-morphing systems for a variety of applications [1-10]. Such “smart” materials are attractive in this context as they can respond to different external stimuli (e.g. electrical/magnetic fields, light irradiation or heat) and can therefore be used to design self-folding structures, which are capable to change their shape without employing external mechanical forces or moments. This ability can be particularly valuable in remote and small-scale devices, such as micro-containers [11], small-scale grippers [12], micro-mirrors [13], deployable solar panels [14], underwater robots [15], micro-robots [16] as well as in wearable [17] and implantable devices [18]. One of the objectives in this field is to design preprogrammed structures to achieve different types of movements such as bending, linear, torsional and even composite motions [16]. This has been achieved, for example, in numerous

origami- and kirigami-inspired structures, which have been built using various active materials (e.g. hydrogels, shape memory alloys and polymers) and actuated using different stimuli (e.g. thermal, electrical, optical, magnetic and chemical) [19-20]. Another effective strategy is based on material anisotropy. This generic concept has been particularly well developed in actuators based on carbon nanotubes (CNTs) [21-22]. In these devices, highly aligned CNTs have been used to achieve a strong anisotropy of the elastic modulus and/or electrical resistance. Because of these anisotropies, they produce different directional motions, depending on the orientation of the CNTs with respect to the device geometry. Inspired by these achievements, here we extend this concept to another class of one-dimensional nanomaterials, which exhibit anisotropic transformation strain when undergoing a phase transition. To this aim, we use spin crossover (SCO) materials, which are transition metal complexes (molecules or coordination networks) displaying reversible switching between the high spin (HS) and low spin (LS) states of the metal ion (most often Fe^{2+}) under an external stimulus [23-29]. Importantly, the change of the spin state of the material is associated typically with 1-10 % volume strain, which can be advantageously used in shape morphing applications [30-31]. In fact, the SCO phenomenon is not only accompanied by a large spontaneous strain [32] and associated working densities (up to a few tens of $J.cm^{-3}$ [31]), but provides also unique multi-responsiveness (to pressure, light, chemical stimuli, temperature or a current via Joule effect). Moreover, these materials present multi-functionality (concomitant change of optical, caloric, magnetic and mechanical properties) and large compositional, morphological and scale versatility [33-35]. To enhance their processability, SCO complexes are frequently obtained as nanoparticles [36] embedded into polymer matrices to form hybrids or nanocomposites [37-38]. To exploit this potential of SCO materials, we have recently developed a series of bilayer bending cantilever devices [39-45]. In these bimorph actuators, the first layer was made of SCO particles embedded in a polymer matrix. This layer served to generate a significant thermal strain, leading to a strain mismatch and subsequent bending of the cantilever. The second layer consisted of silver particles loaded into the same polymer, which was either poly(vinylidene fluoride - trifluoroethylene), P(VDF-TrFE), or thermoplastic polyurethane, TPU. This second layer was electrically conducting and afforded thus for electro-thermal actuation via Joule heating. The devices displayed ample bending motions (up to ~270° curling), high positioning accuracy (>99 %), long service life (>35000 times), low driving voltage (< 3 V) and fast closed-loop response (ca. 2 s), which are promising assets for shape morphing applications. In these previous works, we cut the bilayer films in a U-shape, which is the simplest and most common form of electrical current-driven bending cantilevers. As discussed in ref. 22, such U-shaped actuators can be also

assembled into more complex shapes to realize various directional motions. In the present paper, we investigate T-shaped SCO@TPU/Ag@TPU actuators, which afford for various interesting bending motions by simply controlling the cutting angle of the composite bilayer. We show that the fundamental difference with respect to the CNT-based devices is that the control of the deformation in our SCO actuators stems directly from the anisotropy of the SCO-induced thermal strain, instead of some indirect effects brought in by the anisotropy of mechanical or electrical properties.

Methods

Needle-like, high aspect ratio particles of the SCO complex $[Fe(Htrz)_{1.8}(trz)_1(NH_2trz)_{0.2}](BF_4)_1 \bullet 0.7H_2O$ (**1**) were prepared by a reverse micelle method following the procedure outlined previously in Ref. 41. Isometric SCO nanoparticles of $[Fe(Htrz)_{2.1}(trz)_{0.8}(NH_2trz)_{0.1}](BF_4)_{1.2} \bullet 0.8H_2O$ (**2**) were synthesized via high concentration precipitation as described previously in Ref. 46. The composite films **1**@TPU, **2**@TPU and Ag@TPU were fabricated using a blade casting procedure, outlined in Ref. [45]. T-shaped electrothermal actuators were cut from large-area SCO@TPU/Ag@TPU bilayer films using a Snapmaker A250T laser cutter. Three actuators were cut from the same sheet (for both compounds) in different directions with respect to the cast direction (see Fig. 1a).

Particle size and shape were determined by transmission electron microscopy (TEM) using a JEOL JEM-1011. TEM samples were prepared by placing on a carbon coated copper grid a drop of the particles suspended in ethanol. The SCO properties of the particles were assessed using a Quantum Design MPMS magnetometer under a field of 1 kOe. Scanning electron microscopy (SEM) images of the composite films were acquired using a JEOL JSM 7800F Prime operated at 5 kV. Samples for SEM were prepared by breaking the film cooled by liquid nitrogen and metallizing the cross section with Pt. Dynamic mechanical analysis (DMA) of the SCO@TPU films was performed in tensile mode using a DMA850 from TA Instruments. For the DMA measurements, two rectangular specimens were cut from the same sheet (for both compounds) in parallel and perpendicular orientations with respect to the cast direction. The length, width and height of test samples were ca. 10, 8 and 0.1 mm, respectively. An initial static tensile force of 0.1 N was applied on the samples and was continuously adjusted using the 'force tracking' option to keep it proportional to the stiffness of the sample. DMA data were acquired between 20 and 100 °C at a rate of ± 3 °C/min by applying a sinusoidal strain of 1 Hz in frequency and 0.08 % in amplitude. Electrothermal heating of the T-shaped actuators was achieved by means of a Keithley 2420 source-meter unit. The temperature of the samples was

assessed using a Micro epsilon 640 Thermal Imager infrared camera and their movement was recorded using a video camera (see Fig. 1b).

Finite element analysis (FEA) was performed using the ABAQUS software. The actuator was considered as a bilayer, laminated composite shell with properties given in Table 1. The orientation of the active layer was changed in the lamination (0/45/90°) to reflect the different cuts of the samples. The transformation strains were inserted into the simulation as an extra thermal expansion coefficient for the active layer and a uniform temperature was prescribed over the sample. The shell mesh S4R was applied as implemented in ABAQUS and a nonlinear analysis was performed in order to better reflect the deformed shape of the samples.

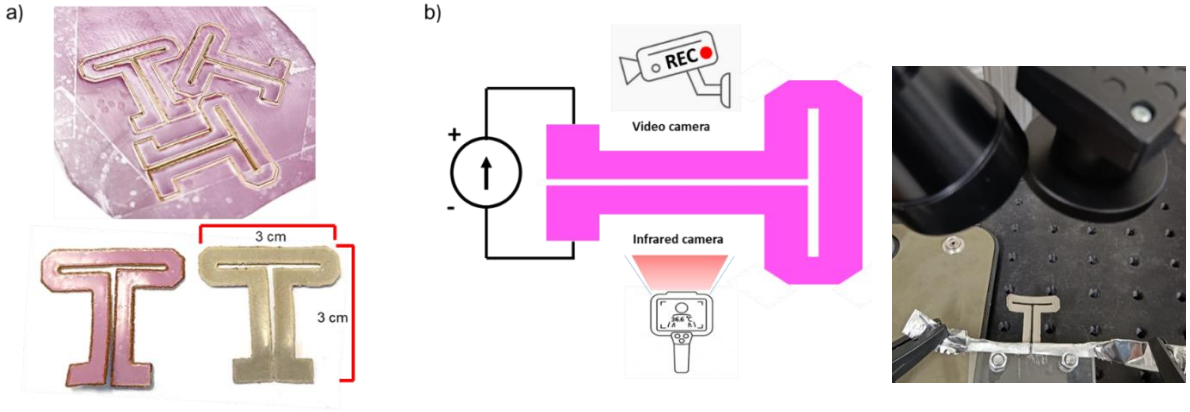

Figure 1. (a) Photographs of the bilayer actuator devices showing also the three cut directions. The SCO@TPU and Ag@TPU layers are pink and silvery, respectively. b) Scheme and photo of the experimental setup incorporating a video camera, an infrared camera and a current source for electro-thermal heating.

Results and discussion

In order to produce composite films with anisotropic thermomechanical properties, needle-shaped SCO particles were synthesized and embedded in a TPU polymer matrix. The latter was chosen for its ease of processability [47-50], but we anticipate that several other polymers should provide similar results. As shown in the TEM images (Fig. 2), the elongated $[Fe(Htrz)_{1.8}(trz)_1(NH_2trz)_{0.2}](BF_4)_1$ (**1**) particles are characterized by a length of ca. 2 µm and an aspect ratio of ca. 30. For comparison, we have also synthesized isometric nanoparticles of $[Fe(Htrz)_{2.1}(trz)_{0.8}(NH_2trz)_{0.1}](BF_4)_{1.2}$ (**2**) with ca. 50 nm mean size (Fig. 2). One can remark that the stoichiometry of the two types of particles is slightly different, but the magnetic susceptibility measurements shown in Fig. 2 confirmed that their SCO properties were closely comparable. As expected for such particle morphologies and sizes, a hysteretic behaviour centred at ca. 70°C is observed [41,46]. Due to the high degree of disorder in the non-stoichiometric compounds **1** and **2**, we could not assess reliably the transformation strain in the

particles by means of powder X-ray diffraction. Nevertheless, in a first approximation, we can suggest that they should have similar properties than the "parent" $[Fe(Htrz)_2(trz)]BF_4$ complex [46]. Indeed, the latter was shown to display ca. 11 % volumetric expansion of the crystalline lattice during the spin transition phenomenon [51]. Importantly, this volume strain was found rather anisotropic, with a ca. 6 % linear expansion upon the spin transition across the length of the rod-shaped crystalline domains.

Using particles of **1** and **2**, as well as commercially available silver flakes, large-scale (10 cm side) SCO@TPU/Ag@TPU bilayer films were prepared using previously described blade casting techniques with ca. 70 wt. % Ag and 25 wt. % SCO particle concentrations. As already reported, such concentrations are optimized for the joule heating effect and the actuation performance of the device, respectively [45]. Figure 3 displays selected SEM cross-section images of composite bilayer SCO@TPU/Ag@SCO films. Figure 3a shows that a quite regular thickness of ca. 200 microns is obtained for the bilayer with similar thicknesses for both layers. The separation of the conductive Ag@SCO and the actuating SCO@TPU layers is neat. Let us stress here the importance to use the same polymer backbone, which permits to maintain the mechanical integrity of the bilayer. Indeed, with this type of monolithic structures we have never met delamination problems.

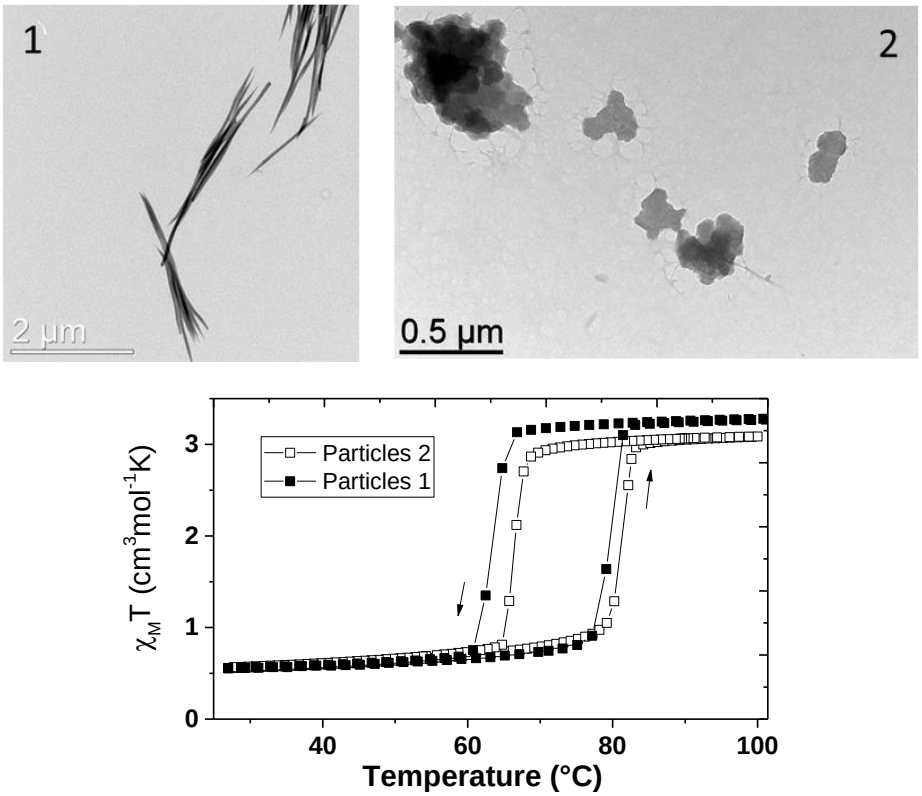

Figure 2. Top panel: Representative TEM images of the SCO particles **1** and **2**. Bottom panel: Product of molar magnetic susceptibility and temperature measured on heating and cooling (shown by arrows) during the 2nd thermal cycle for the powders of **1** and **2**.

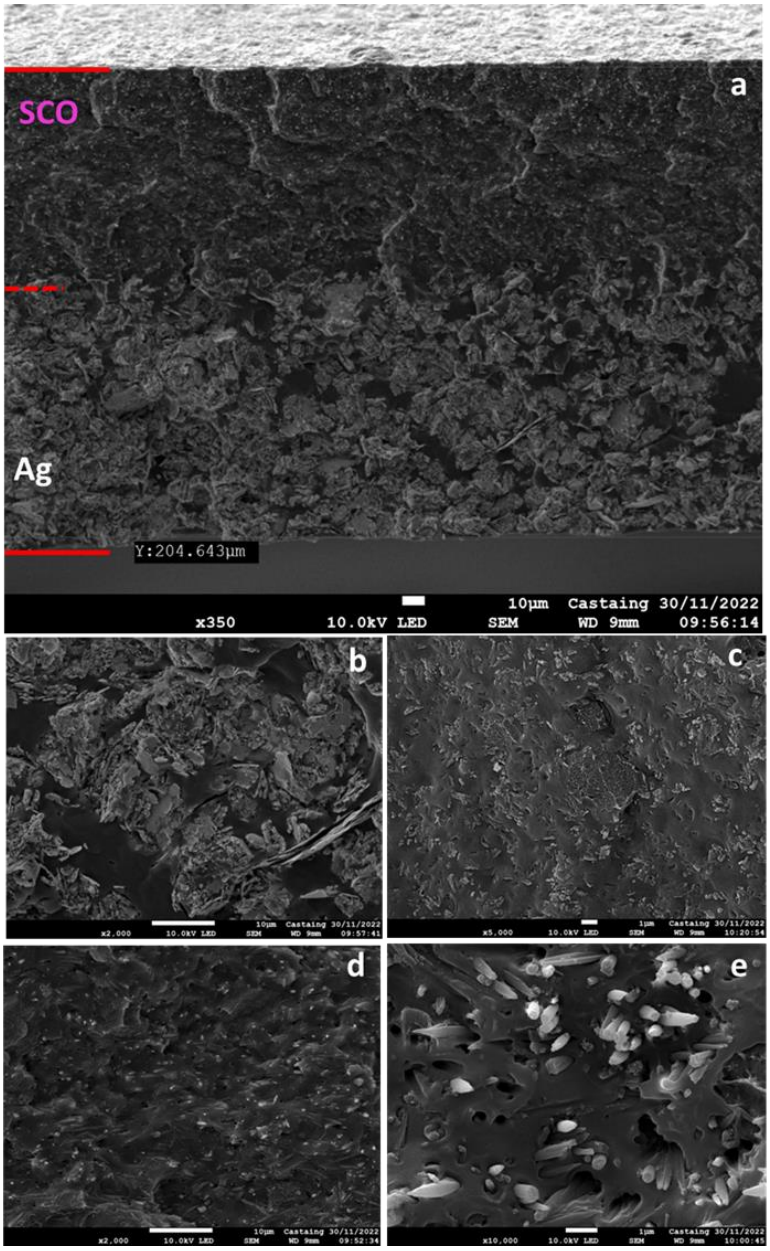

Figure 3. Representative SEM images of the cross-sections of the composite films: (a) **1**@TPU/Ag@TPU, (b) Ag@TPU, (c) **2**@TPU, (d) **1**@TPU// and (e) **1**@TPU⊥.

The zoom on the Ag@SCO layer in Figure 3b reveals more clearly the silver flakes of ca. 10 microns size in the composite, whereas in the SEM image of the **2**@TPU layer we can distinguish aggregated quasi-spherical nanoparticles of compound **2** (Fig. 3c). To confirm whether the needle-like anisometric particles **1** are aligned in the composite **2**@TPU film, we compared SEM images with parallel (Fig. 3d) and orthogonal (Fig. 3e) cross-sections with

respect to the cast direction. For the parallel cross-section (**1**@TPU//), we can depict several entire needles, while for the orthogonal cross-section (**1**@TPU⊥) we can see most often just the needle sections. We can thus conclude that the needles **1** have been preferentially aligned during the film casting, which was also confirmed by the observed anisotropy of the transformation strain (*vide infra*).

Finally, from the bilayer films T-shaped actuators were cut, which will be denoted **A1** for the anisometric and **A2** for the isometric particles. Cuts were made from each bilayer in three different directions: the long axis of the T-shaped device being either parallel (**A1-0°** and **A2-0°**) or perpendicular (**A1-90°** and **A2-90°**) or diagonal (**A1-45°** and **A2-45°**) with respect to the film casting direction (see Fig. 1a). This way we ensure that differences between the device properties come primarily from the different SCO particle orientation, i.e. from the different orientations of the axes of anisotropy of the SCO@TPU layer vs. the device axes. Indeed, the T-shaped geometry of the actuators allows us to evaluate the bending of the bilayer material caused by the expansion mismatch between the two layers, simultaneously in two different axes, making it easier to visualize the effect of anisotropy. In this respect, actuators **A2** with the isometric particles serve as a witness, which should provide negligible directional response.

To investigate the deformation behavior of the devices they were actuated electro-thermally under open-loop conditions (using a maximum current of 1.1 A) and the resulting temperature rise and bending movement were recorded using an IR and a video camera, respectively (Fig 1b). As shown in Figure 4, the anisotropic **A1** actuators showed very significant deformations upon the spin transition. The movement was usually reversible, though in some cases a slight residual deformation occurred, which can be attributed to plastic deformation of the TPU matrix. As it can be expected for a highly anisotropic composite, the actuation in the three T-shaped devices shows dissimilar forms and can thus provide multiple functionalities. Actuator **A1-90°** shows symmetrical bending of its shorter axis, which can be assimilated to a gripper (Fig. 4a). The device **A1-0°** works as a cantilever with a pronounced bending along its long axis (Fig. 4b). As for the diagonal cut system **A1-45°**, it curls up upon thermal stimulation and then unfolds when the heating is switched off. Thermal imaging showed quite similar heating profiles for the different actuators, independently of the cut direction, proving that the observed anisotropy in the movement of the actuator does not come from different temperature distributions. As an example, Figure 5 shows temperature maps of actuator **A1-0°** wherein we can see that the non-clamped end of the actuator reaches somewhat higher temperatures than the clamped end, denoting a temperature gradient along the long axis of the device, as it can be expected for this type of single clamping mode. In the case of actuators

A2, there is almost no motion upon heating, independently of the cut direction (Fig. 4d-e). Despite the fact that the samples are heated above the spin transition temperature, the isotropic actuators do not exert enough force to lift their own weight and thus, no movement is observed. The fact that using almost identical SCO materials with different particle morphologies leads to vastly different results suggests thus that the particle orientation induced anisotropy plays a key role in the actuation of these devices.

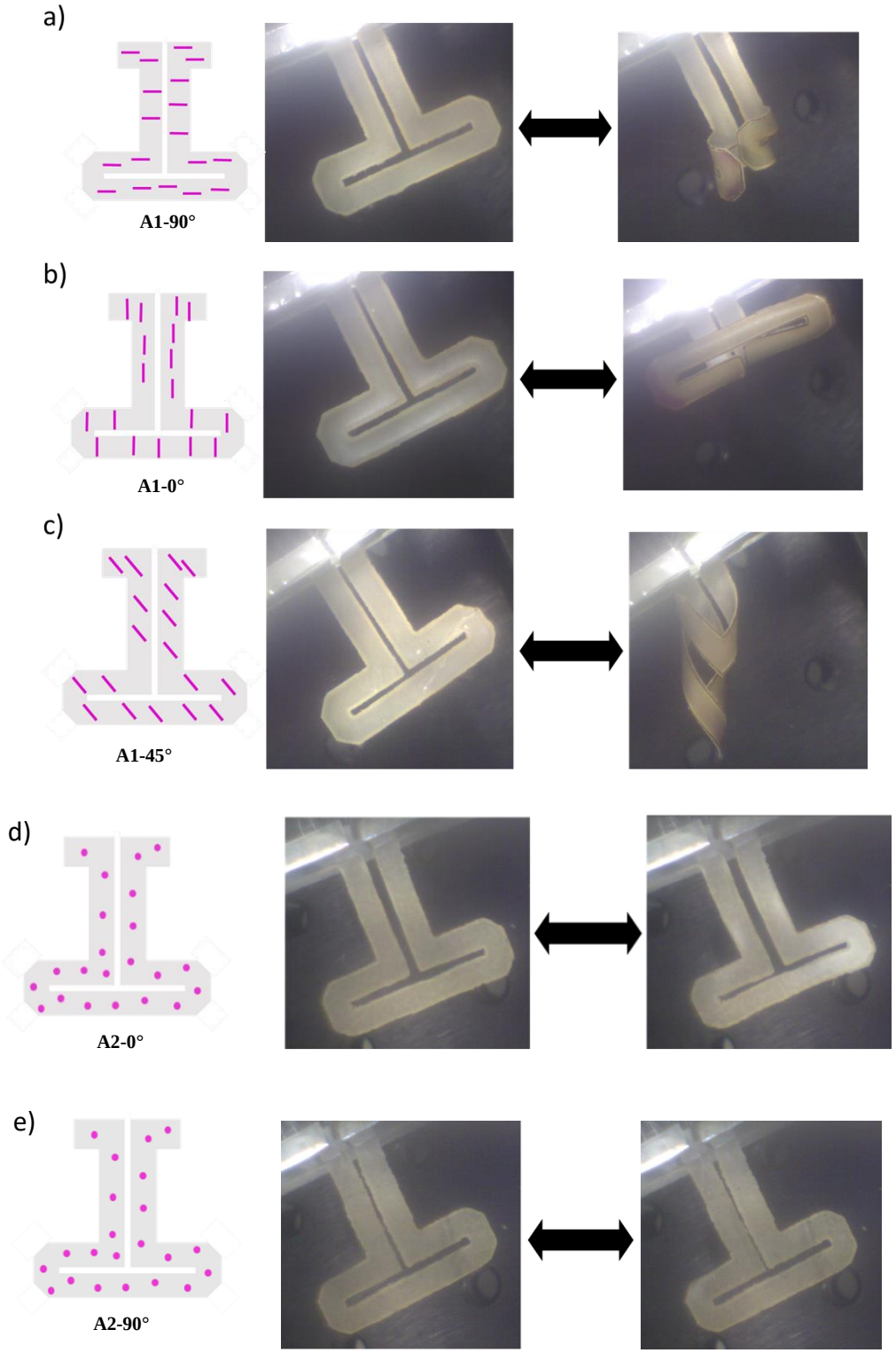

Figure 4. Reversible, electro-thermally driven motion of actuators **A1-90°** (a), **A1-0°** (b), **A1-45°** (c), **A2-0°** (d) and **A2-90°** (e). The schemes show the cut directions of the actuators relative to the direction of the casting and the resulting orientation of the particles.

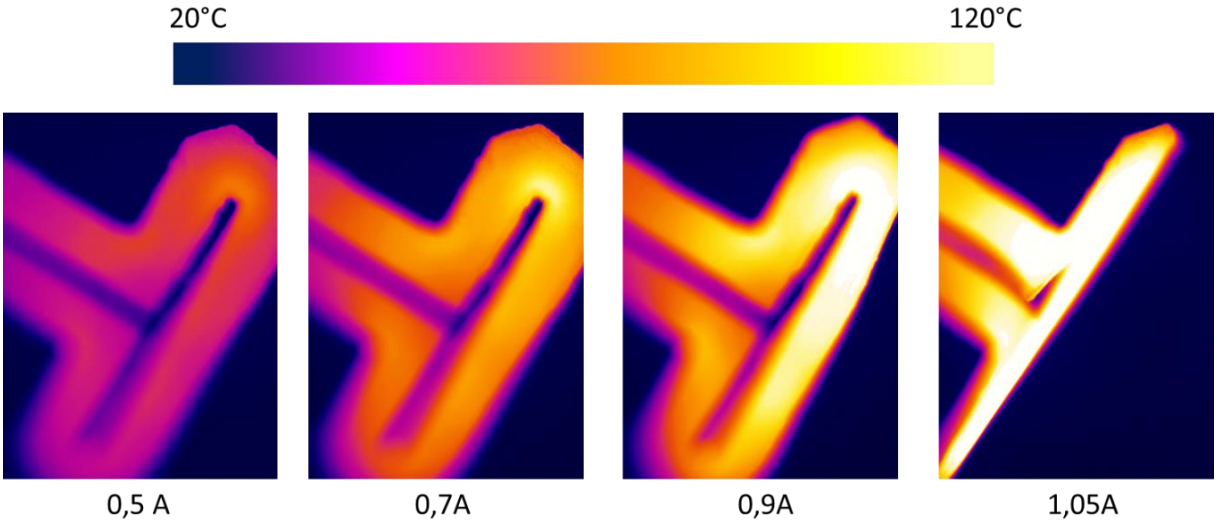

Figure 5. Temperature distribution in the actuator **A1-0°** for selected current excitation values between 0.5 and 1.05 A.

In order to understand the origin of the peculiar bending motions in our actuators, we conducted a combined experimental and theoretical analysis of their actuation behavior using dynamical mechanical analysis (DMA) and finite element analysis (FEA). DMA measurements were performed on the two composite films, cut either in parallel (**1**@TPU// and **2**@TPU//) or in perpendicular (**1**@TPU⊥ and **2**@TPU⊥) orientations with respect to the film casting direction. As it can be expected, the real part of the dynamic elongation modulus (i.e. the storage modulus, *E'*) of the composites was found more reinforced by the elongated particles **1** when compared to the isometric ones (see Table 1). On the other hand, rather surprisingly, the 'perpendicular-cut' samples turned out to be stiffer, even for the case of the isometric particles. This finding indicates that the film casting process might introduce some anisotropy to the elastic properties of the films. The impact of the particle shape and orientation appears strikingly in the thermal expansion properties of the composites, which was also assessed from the DMA data. As shown in Figure 6, far from the spin transition temperatures, the films show ordinary thermal expansion behaviors, characterized by linear thermal expansion coefficients (α) of ~10^{-4} °C^{-1}. At the spin transition temperatures, ca. 85 °C on heating and 55 °C on cooling, abrupt expansion and contraction occurs, respectively, denoting a thermal hysteresis of the strain. (At this point, it may be worth to note that the hysteresis depicted in the DMA experiment in Fig. 6 is larger

when compared to the magnetic measurements in Fig. 2, but this reflects merely a higher thermal lag in the former.) The transformation strain (ε^T) associated with the spin transition can be then defined as the difference of strain between the heating and cooling modes at the barycenter of the hysteresis loop (i.e. at 70 °C). The composite **2**@TPU shows ca. 0.7-0.8 % strain upon spin transition, the difference between the two cut directions being comparable with the experimental uncertainty, in agreement with the fact that there is no preferential orientation of the isometric particles in this sample. On the other hand, the composite **1**@TPU exhibits not only higher transformation strain, but also a marked anisotropy of the strain between the perpendicular and the parallel directions (1.2 vs. 1.7 %, respectively), as it can be expected for anisotropic compounds with a high degree of particle alignment.

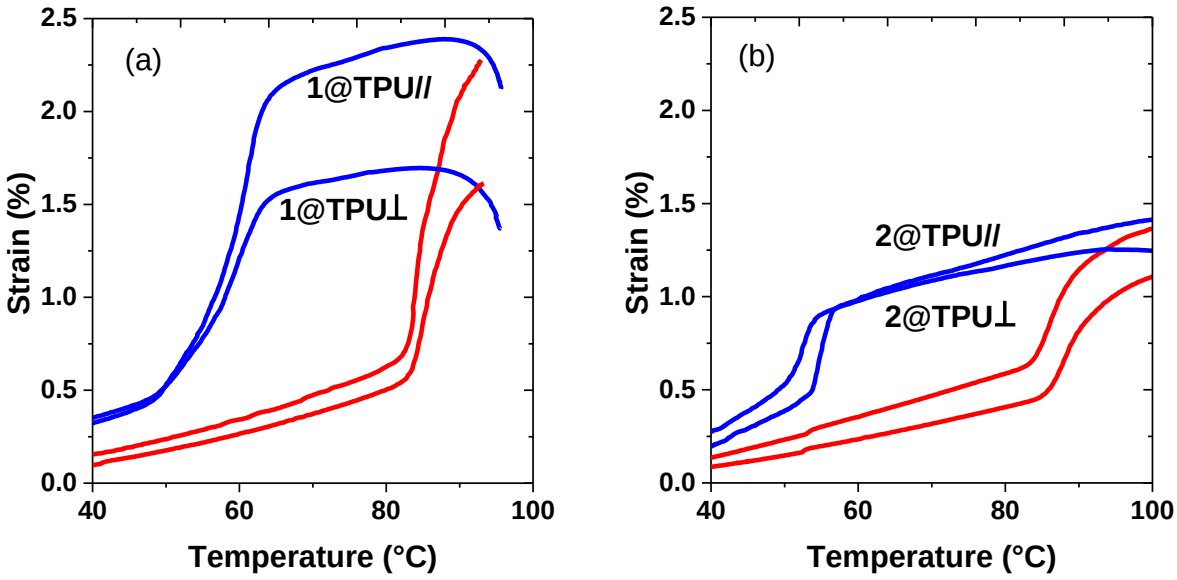

Figure 6. Thermal expansion of the composite films **1**@TPU (a) and **2**@TPU (b), cut either in parallel (//) or in perpendicular (⊥) orientation with respect to the film casting direction. Data were recorded during the second thermal cycle on heating (red) and cooling (blue).

The role of the different material properties cannot be unequivocally discussed based on the experimental data, because several parameters change concomitantly from sample to sample. To refine the analysis and provide a clear picture about the interplay between the actuator movement and the material properties, we have carried out a series of finite element simulations using the commercial ABAQUS software. The geometries and thermomechanical properties of the simulated actuators are given in Table 1. We have considered the device to be clamped at the bottom boundary and the two layers (Ag@TPU and SCO@TPU) are modeled as a laminate

with given mechanical and thermal expansion properties. To simplify the analysis the temperature of the device was considered homogeneous and the ordinary thermal expansion coefficient was taken as 10^{-4} °C^{-1} for all layers. The deformed shape of the actuators **A1-90°**, **A1-0°** and **A1-45°** are shown in the top panel of Figure 7. The comparison between the simulation results and the experimentally observed deformed shapes in Figure 4 shows a reasonably good agreement, validating thus the numerical approach.

Table 1. Geometry and mechanical properties of the samples used in the FEA simulations. (The elastic modulus and transformation strain values were taken at 70 °C.)

Layer	Thickness (μm)	E'// (MPa)	E'⊥ (MPa)	ε^T// (%)	ε^T⊥ (%)
Ag@TPU	110	50	50	0	0
1@TPU	95	85	160	1.7	1.2
2@TPU	95	6	30	0.7	0.8

In the next step, we changed one-by-one the different material parameters in the simulations in order to explore their respective role. To this aim, we have focused on the actuator **A1**. To examine the effect of the anisotropy of the elastic modulus we set the values of the in-plane elastic moduli equal to E'// = E'⊥ = 160 MPa. A comparison of the simulated bending behaviors with isotropic and anisotropic in-plane moduli in Fig. 7 (2nd and 1st row, respectively) reveals no substantial differences, indicating that the mechanical anisotropy has only a minor role in the observed deformation of the actuator. In a similar way, we then set the in-plane transformation strain values equal to ε^T// = ε^T⊥ = 1.7 %. . As shown in Figure 7, the isotropic strain gives rise to a bending behavior, which is dramatically different in comparison with the case of anisotropic strain (3rd and 1st row, respectively). Indeed, due to the needle shape of the particles **1**, depending on their orientation, different deformations will arise in the x-y directions of the plane of the device, which results in various possible bending modes. On the other hand, if there is no strain anisotropy, which is the case of the film **2**@TPU with isometric particles, bending of the actuator occurs along its long axis with a simultaneous bending along the short axis as well – independently of the cut direction. Obviously, the magnitude of the transformation strain is directly correlated with the bending amplitude (see the 3rd and 4th rows in Fig. 7). However, it is important to recognize that the anisotropy of the transformation strain

gives rise an enlarged deformation of the samples because of the coupling of the axial and bending deformations, which occurs only in the anisotropic samples.

	Cut direction: 90°	Cut direction: 0°	Cut direction: 45°
Parameters from Table 1:	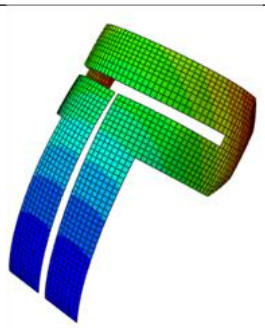	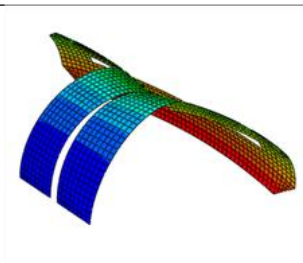	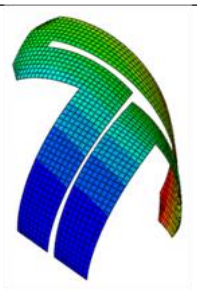
Parameters from Table 1, but with isotropic modulus: E'// = E'⊥= 160 MPa	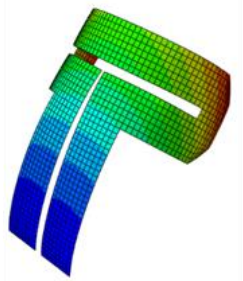	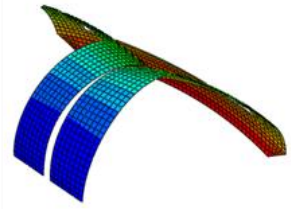	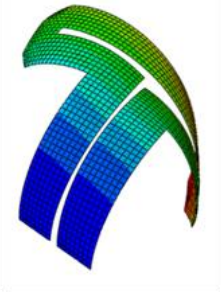
Parameters from Table 1, but with isotropic transformation strain: ε^T // = ε^T⊥ = 1.7 %	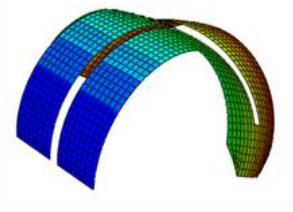	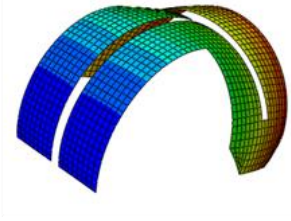	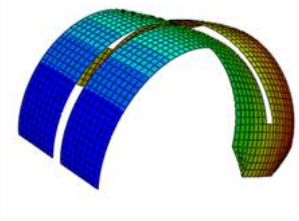
Parameters from Table 1, but with small and isotropic transformation strain: ε^T // = ε^T⊥ = 0.7 %	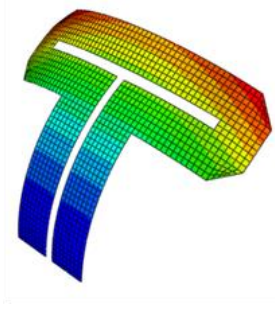	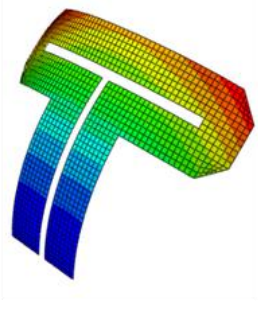	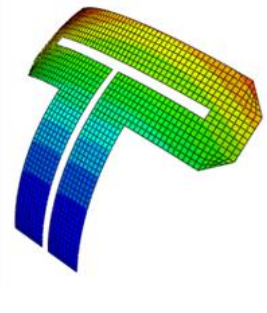

Figure 7. FEA simulations of the thermally induced deformations of the bilayer actuators **A1** with particles oriented perpendicular (90°), parallel (0°) or diagonal (45°) with respect to the long axis of the T-shaped device. Top row: simulated behavior of the devices with parameters

from Table 1. In the other rows, the simulated parameters were changed to isotropic elastic modulus (2nd row), isotropic transformation strain (3rd row) and small, isotropic transformation strain (4th row).

Conclusions

In summary, we investigated a new type of bilayer actuators, which can realize various pre-programmed deformations upon electro-thermal stimulation. Based on FEA simulations, the encoded motion of the actuators can be pre-designed 'on demand' by adjusting the thermomechanical and geometrical properties of the structure. Contrary to previously reported devices, the deformation type of the present actuators stems directly from the anisotropy of the transformation strain, which is imparted by the oriented, anisometric spin crossover particles used in the construction of the stimuli-responsive layer. This asset provides access to novel functionalities and unprecedented combination of properties via specific actuator geometries, broadening the applicability of these devices.

Acknowledgments

This project has received funding from the European Research Council (ERC) under the European Union's Horizon 2020 research and innovation programme (grant agreement No. 101019522). XY thanks the China Scholarship Council for a PhD grant.

Conflicts of Interest

The authors declare no conflicts of interest.

References

[1] M. Liu, L. Jin, S. Yang, Y. Wang, C. B. Murray, S. Yang, Adv. Mater. 35 (2023) 2208613

[2] A. S. Gladman, E. A. Matsumoto, R. G. Nuzzo, L. Mahadevan, J. A. Lewis, Nat Mater. 15 (2016) 413–418

[3] M. Li, A. Pal, A. Aghakhani, A. Pena-Francesch, M. Sitti, Nat. Rev. Mater. 7 (2022) 235.

[4] E. Hajiesmaili, D. R. Clarke, Nat. Commun. 10 (2019) 183.

[5] I. Apsite, S. Salehi, L. Ionov, Chem. Rev. 122 (2022) 1349.

[6] G. Constante, I. Apsite, H. Alkhamis, M. Dulle, M. Schwarzer, A. Caspari, A. Synytska, S. Salehi, L. Ionov, ACS Appl. Mater. Interfaces 13 (2021) 12767−12776.

[7] V. P. Anju, R. Pratoori, D. K. Gupta, R. Joshi, R. K. Annabattula, P. Ghosh, Soft Matter. 16 (2020) 4162.

[8] Y. Wang, M. Li, J.-K. Chang, D. Aurelio, W. Li, B. J. Kim, J. H. Kim, M. Liscidini, J. A. Rogers, F. G. Omenetto, Nat. Commun. 12 (2021) 1651.

[9] Q. Guo, J. Yan, C. Wu, J. Jiang, J. Zhou, Z. Lin, N. Hua, P. Zhang, C. Zheng, K. Yang, M. Weng, ACS Appl. Mater. Interfaces 14 (2022) 49171−49180.

[10] L. Ren, B. Li, K. Wang, X. Zhou, Z. Song, L. Ren, Q. Liu, Front. Matt. 8 (2021) 651521.

[11] P. H. Pham, D. V. Dao, S. Amaya, R. Kitada, S. Sugiyama, J. Micromech. Microeng. 16 (2006) 2532.

[12] S. Zaidi, M. Maselli, C. Laschi, M. Cianchetti, Current Robotics Reports 2 (2021) 355.

[13] Y. Tang, J. Li, L. Xu, J.-B. Lee, H. Xie, Micromachines 13 (2022) 429.

[14] Y. Li, Y. Zhao, Y. Chi, Y. Hong, J. Yin, Materials Today Energy 22 (2021) 100874.

[15] H. Shahsavan, A. Aghakhania, H. Zeng, Y. Guo, Z. S. Davidson, A. Priimagi, M. Sitti, Proc. Natl. Acad. Sci. U. S. A. 117 (2020) 5125–5133.

[16] H. Kim, S.-k. Ahn, D. M. Mackie, J. Kwon, S. H. Kim, C. Choi, Y. H. Moon, H. B. Lee, S. H. Ko, Material Today 41 (2020) 243.

[17] Y. Chen, Y. Yang, M. Li, E. Chen, W. Mu, R. Fisher, R. Yin, Textiles 1 (2021) 283.

[18] F. A. Hassani, W. Y. Xian Peh, G. G. Lasam Gammad, R. P. Mogan, T. Kiat Ng, T. L. Chuen Kuo, L. Guat Ng, P. Luu, S.-C. Yen, C. Lee, Adv. Sci. (2017) 1700143.

[19] Y.-C. Cheng, H.-C. Lu, X. Lee, H. Zeng, A. Priimagi, Adv. Mater. 32 (2020) 1906233.

[20] J. Na, A. A. Evans, J. Bae, M. C. Chiappelli, C. D. Santangelo, R. J. Lang, T. C. Hull, R. C. Hayward, Adv. Mater. 27 (2015) 79–85.

[21] J. Deng, J. Li, P. Chen, X. Fang, X. Sun, Y. Jiang, W. Weng, B. Wang, H. Peng, J. Am. Chem. Soc. 138 (2016) 225−230.

[22] Q. Li, C. Liu, Y.-H. Lin, L. Liu, K. Jiang, S. Fan, ACS Nano 9 (2015) 409.

[23] K. S. Kumar, M. Ruben, Angew. Chem. Int. Ed. 60 (2021) 7502.

[24] M. Halcrow, I. Capel Berdiell, C. M. Pask, R. Kulmaczewski, Inorg. Chem. 58 (2019) 9811−9821.

[25] N. T. Madhu, E. T. Knittl, T. D. Zeleke, A. G. Robi, W. Linert, J. Chem. Appl. Chem. Eng. (2017) 1:2.

[26] M.-L. Boillot, B. Weber, C. R. Chimie 21 (2018) 1196.

[27] H. L.C. Feltham, A. S. Barltrop, S. Brooker, Coord. Chem. Rev. 344 (2017) 26.

[28] O. Shakirova, L. Lavrenova, Crystals 10 (2020) 843.

[29] M. C. Munoz, J. A. Real, Coord. Chem. Rev. 255 (2011) 2068.

[30] H. Shepherd, I. Gural'skiy, C. Quintero, S. Tricard, L. Salmon, G. Molnar and A. Bousseksou, Nat. Commun. 4 (2013) 2607.

[31] M. D. Manrique-Juarez, S. Rat, L. Salmon, G. Molnar, C. M. Quintero, L. Nicu, H. J. Shepherd, A. Bousseksou, Coord. Chem. Rev. 308 (2016) 395–408.

[32] P. Guionneau, Dalton Trans. 43 (2014) 382-393.

[33] Spin Crossover in Transition Metal Compounds I-III, ed. P. Gütlich and H. A. Goodwin, Springer, Berlin, Heidelberg, Germany, 2004.

[34] Spin-Crossover Materials: Properties and Applications, ed. M. A. Halcrow, John Wiley & Sons Ltd, Oxford, UK, 2013

[35] Spin crossover phenomenon, ed. A. Bousseksou, C. R. Chimie 21 (2018) 1055–1300.

[36] L. Salmon, L. Catala, C. R. Chimie 21 (2018) 1230.

[37] A. Enriquez-Cabrera, A. Rapakousiou, M. Piedrahita Bello, G. Molnár, L. Salmon, A. Bousseksou, Coord. Chem. Rev. 419 (2020) 213396.

[38] J. E. Angulo-Cervera, M. Piedrahita-Bello, B. Martin, S. E. Alavi, W. Nicolazzi, L. Salmon, G. Molnar, A. Bousseksou, Mater. Adv. 3 (2022) 5131.

[39] I. A. Guralskiy, C. M. Quintero, J. Sa´nchez Costa, P. Demont, G. Molnar, L. Salmon, H. J. Shepherd and A. Bousseksou, J. Mater. Chem. C 2 (2014) 2949–2955.

[40] M. D. Manrique-Juarez, F. Mathieu, A. Laborde, S. Rat, V. Shalabaeva, P. Demont, O. Thomas, L. Salmon, T. Leichle, L. Nicu, G. Molna´r and A. Bousseksou, Adv. Funct. Mater. 28 (2018) 1801970.

[41] M. Piedrahita-Bello, J. E. Angulo-Cervera, A. Enriquez-Cabrera, G. Molnar, B. Tondu, L.Salmon, A.Bousseksou, Mater. Horiz. 8 (2021) 3055.

[42] M. Piedrahita-Bello, Y. Zan, A. Enriquez-Cabrera, G. Molnar, B. Tondu, L. Salmon, A. Bousseksou, Chem. Phys. Lett 793 (2022) 139438.

[43] M. Piedrahita-Bello, J. E. Angulo-Cervera, R. Courson, G. Molnar, L. Malaquin, C. Thibault, B. Tondu, L. Salmon, A. Bousseksou, J. Mater. Chem. C 8 (2020) 6001.

[44] B. Tondu, M. Piedrahita-Bello, L. Salmon, G. Molnár, A. Bousseksou, Sens. Actuators A 335 (2022) 113359.

[45] Y. Zan, M. Piedrahita-Bello, S. E. Alavi, G. Molnár, B. Tondu, L. Salmon, A. Bousseksou, Adv. Intell. Syst. (2023) 2200432.

[46] M. Piedrahita-Bello, K. Ridier, M. Mikolasek, G. Molnar, W. Nicolazzi, L. Salmon, A. Bousseksou, Chem. Commun. 55 (2019) 4769.

[47] H. Liu, F. Wang, W. Wu, X. Dong, L. Sang, Composites Part B 248 (2023) 110382

[48] H. Dong, J. Sun, X. Liu, X. Jiang, S. Lu, ACS Appl. Mater. Interfaces 14 (2022) 15504.

[49] Y. He, J. Guo, X. Yang, B. Guo, H. Shen, RSC Adv. 11 (2021) 37744.

[50] X. Ji, F. Gao, Z. Geng, D. Li, Polymer Testing 97 (2021) 107135.

[51] A. Grosjean, P. Négrier, P. Bordet, C. Etrillard, D. Mondieig, S. Pechev, E. Lebraud, J. -F. Létard, P. Guionneau, Eur. J. Inorg. Chem. (2013) 796.